



Cite this: *Mater. Adv.*, 2025,
6, 3605

Low-temperature APPJ printing of Kesterite on flexible substrates for heterojunction solar cells†

M. Dhanasekar,^{‡,a} Stenny Benny,^a Avishek Dey, ^{ID}^{*bc} Satheesh Krishnamurthy^{*bd} and S. Venkataprasad Bhat^a

Kesterite $\text{Cu}_2\text{ZnSnS}_4$ (CZTS), composed of earth-abundant, non-toxic elements, is considered a promising chalcogenide photoabsorber. One of the major roadblocks in its large-scale implementation is limited scalability for roll-to-roll fabrication at low temperatures. Herein, we reported an ambient-air deposition method for CZTS films onto rigid as well as flexible surfaces at a low temperature (~ 170 °C) and tested their applicability in heterojunction solar cells. In this process, the precursor solution was directly coated onto conductive substrates using an atmospheric pressure plasma jet (APPJ). The rich chemistry of APPJ was used to engineer the surface energy of the substrates, while the charged particles, neutral metastable species, and radicals were used to activate reactions that were thermodynamically unfavorable under ambient conditions. Here, we carefully controlled a high temperature in the plasma while maintaining a low temperature at the substrate. This open-air processing overcame the complex and high-temperature (~ 500 °C) requirements for controlled sulfurization or selenisation. By employing an environmentally benign molecular precursor made with a green solvent, our method aligned well with the increasing demand for industry-relevant, eco-friendly manufacturing processes. The plasma-printed CZTS showed p-type characteristics and a band gap in the visible region. As a proof of concept, we measured the power conversion efficiencies (PCEs) of functional CZTS/CdS heterojunction solar cells on both rigid ITO substrates ($\sim 3.1\%$) and flexible ITO substrates ($\sim 1.1\%$). The measured PCEs set new benchmarks for low-temperature-processed CZTS devices. Through favourable engineering of interfacial layers and the integration of passivation layers, higher efficiency and stability could be achieved.

Received 7th March 2025,

Accepted 13th April 2025

DOI: 10.1039/d5ma00207a

rsc.li/materials-advances

1. Introduction

Metal chalcogenides are recognized as promising candidates for the absorber material in the advancement of cost-effective thin-film solar cells.^{1,2} $\text{Cu}_2\text{ZnSnS}_4$ (CZTS) has emerged as a green replacement option for CdTe and CIGS in thin-film solar cells, owing to its high absorption coefficient (10^4 cm⁻¹), optimum band gap (E_g) (1.0–1.5 eV), and earth-abundant, environmentally friendly constituents.^{3–5} Recently, considerable advancements have been made in this material's PCE, attaining up to 14.9%.^{6–12} Several deposition techniques have been employed to prepare CZTS films,

such as thermal, co-evaporation,¹³ electrodeposition,¹⁴ sputtering,¹⁵ and solution-based techniques.¹⁶ In particular, low-temperature solution processing of CZTS is being pursued to facilitate the scalable and low-cost fabrication of thin-film solar cells on both rigid and flexible substrates.^{11,17–19} However, the toxicity of solvents used and the high-temperature annealing processes required for fabricating high quality absorbers are major hindrances to making it compatible with large-scale, low-cost manufacturing.^{2,20,21} Several non-toxic solvent-based precursor solutions or inks for making CZTS films have been explored using dimethyl sulfoxide (DMSO), ethanol, *N,N*-dimethyl formamide (DMF), 2-methoxyethanol, and 1,3-dimethyl-2-imidazolidinone (DMI).^{21–27} However, a high-temperature annealing process is generally required to reduce the impurity phases (CuS, ZnS, and SnS) and achieve better crystalline quality of the CZTS film on both rigid and flexible substrates.^{2,20,21,28–30} For instance, a sulfurization temperature of 550 °C on a rigid substrate was advantageous for the crystal development of CZTS, and its primary effects on the electrical, photovoltaic, and morphological characteristics were analyzed by Payne *et al.*²⁸ A sol-gel process-based CZTS formed on molybdenum (Mo) foil at 500 °C resulted in a device with a PCE of 2.25%, and electrochemically deposited CZTS gave a PCE of

^a Green Energy Materials (GEM) Laboratory, Department of Physics and Nanotechnology, SRM Institute of Science and Technology, Kattankulathur, Tamil Nadu 603 203, India. E-mail: venkatab@srmist.edu.in

^b School of Engineering and Innovation, The Open University, Milton Keynes, MK7 6AA, UK. E-mail: a.dey@ucl.ac.uk, s.krishnamurthy@surrey.ac.uk

^c London Centre for Nanotechnology, University College London, UK

^d Surrey Ion Beam Centre, Advanced Technology Institute, University of Surrey, UK

† Electronic supplementary information (ESI) available. See DOI: <https://doi.org/10.1039/d5ma00207a>

‡ Current address: Department of Physics, SRM Institute of Science and Technology, Ramapuram, Tamil Nadu, India, 600089.



3.82%.^{29,30} CZTS particles were printed on Mo-coated aluminum foil/flexible polyimide substrates to make devices with a PCE of 1–1.94%.^{30,31} A polyimide (PI) substrate-based device was reported by Romero *et al.*,³² where the fabrication of kesterite (CZTS) required a high temperature (~ 490 °C), similar to the other examples mentioned above.

It is worth noting that most of these reports on flexible devices still require an annealing process at high temperatures, and thus use Mo-coated Al foil,³⁰ Ti foil,³³ stain less steel foil, flexible glass (FG, corning willow glass),³⁴ or polyimide (PI) substrates.³² Such rigorous processing conditions could hinder their future advancement, predominantly in devices with flexible formats involving polymer substrates. A few of the reported low-temperature process-based devices were inferior in terms of efficiency compared to those based on high-temperature processing.^{32,35–43} The efficiency reduction primarily stems from charge recombination occurring at flawed interfaces and the presence of structural or chemical defects within the CZTS film. For example, the low-temperature processed glass/ITO/CZTS/CdS/Al devices showed a PCE of 1.34% to 1.85%.^{40,44} Further, Saha *et al.*⁴⁵ introduced an additional layer of Ag-doped CZTS at the interface of CZTS/CdS to improve the depletion region architecture and carrier collection. Farinella *et al.*⁴⁴ reported a good-quality CZTS thin film made *via* electrochemical deposition on flexible PET/ITO substrates at room temperature, but no device was fabricated. Recently, Dhanasekar *et al.* fabricated a dip-coated CZTS absorber on a flexible (PET/ITO) substrate with low-temperature annealing in an argon (Ar) atmosphere, resulting in a device exhibiting a PCE of up to 0.74%.^{46,47} Further exploration in this direction is highly desired to achieve more efficient devices for flexible electronics applications.

Printed and flexible electronics have expanded into many domains, including photovoltaics. The most common printing techniques for solution-processed thin films are inkjet printing⁴⁸ and aerosol printing.⁴⁹ However, both of these approaches require a sintering step or post-thermal annealing to form a thin film. Atmospheric pressure plasma jet (APPJ) is a printing technology that uses atmospheric pressure cold plasma to deposit materials onto a substrate. It can be used to print high-quality materials at low temperatures and in open atmospheres using precursor solutions. The quality and integrity of the film can be improved with this plasma-based process due to the increase in surface tension and wetting properties of the precursor solution. The rich physical and chemical properties of APPJ,⁵⁰ suitable for applications in material processing, healthcare, nanotechnology, and medicine, are widely being explored.⁵¹ APPJ can be utilized for printing nano-colloid inks while simultaneously tuning the surface chemistry and electronic properties of the material being printed. For example, it can reduce highly acidic graphene oxide to graphene *in situ* without the need for any external post-processing.⁵² High-capacity graphite anodes based on APPJ have been studied for the environmentally friendly reuse of lithium-ion batteries.⁵³ Inspired by these observations, we sought to explore the APPJ technique to print the nanocrystalline CZTS solar absorber at

low temperatures under open atmosphere. An environmentally friendly molecular precursor solution was used for the APPJ printing of nanocrystalline CZTS, and simple heterojunction solar cells were fabricated on both rigid and flexible substrates to demonstrate the device application. The results were compared with those obtained using the dip-coated CZTS film annealed under an Ar atmosphere, as well as with other relevant reports from the literature.

2. Experimental section

2.1. Materials

Copper chloride, zinc acetate dihydrate, cadmium chloride monohydrate, propylamine, butylamine, thioacetamide (TAA), and thiourea were purchased from Sisco Research Laboratories Pvt. Ltd. (SRL). Tin chloride dihydrate and 2-methoxyethanol were obtained from Alfa Aesar. Gold was purchased from GRT Gold Jewellery, Chennai, India. Indium-doped tin oxide (ITO) and polyethylene terephthalate (PET)/ITO were procured from Global Nanotech, India. Ethanol, isopropyl alcohol (IPA), and deionized (DI) water were used for cleaning the substrates. The chemicals were used without any additional purification steps.

2.2. Preparation of precursor solution of CZTS

10 mL of 2-methoxyethanol was used to gradually dissolve 1.88 g of copper chloride, 2.19 g of zinc acetate dihydrate, 1.8 g of tin chloride dihydrate, and 4.8 g of thioacetamide at room temperature. The composition ratio of Cu, Zn, Sn, and S was kept within a suitable range: Zn/Sn = 1.25, S/(Cu + Zn + Sn) = 1.88, and Cu/(Zn + Sn) = 0.8.^{54,55} The concentration of the precursor solution was varied according to the requirements for the coating, and a 50% dilution with additional solvent was optimal for APPJ printing.

2.3. APPJ printing and dip coating of CZTS film

APPJ was generated using a quartz nozzle connected to a 15 kV nanosecond pulse generator. Helium gas was used as the carrier gas. A specially designed Teflon nebulizer was used to create an aerosol of the precursor solution, which was generated using the He gas flow. This aerosol was then fed into the plasma and deposited onto the substrate *via* the plasma plume/jet. The operational condition parameters optimized for the APPJ printing of CZTS film were as follows: the diameter of the quartz tube nozzle was 150 μ m; the gas flow was 6 sccm; the input frequency was 40 kHz; and the attenuation was 5×10^{-1} dB km⁻¹.⁵² The precursor solution concentration (50% dilution) and the drying conditions for the film were optimized. A good-quality film was obtained after drying the APPJ-printed CZTS film at 170 °C in an open atmosphere. Additionally, a CZTS film was developed by dip-coating the undiluted precursor solution, drying it at 130 °C, and then annealing it for 2.5 h at 100 °C in an Ar atmosphere (Fig. S1–S3, ESI†). The results obtained from this dip-coated film were compared with those produced using the APPJ technique. A schematic of APPJ printing of CZTS film for the fabrication of solar cells on rigid and flexible substrates is shown in Fig. 1.

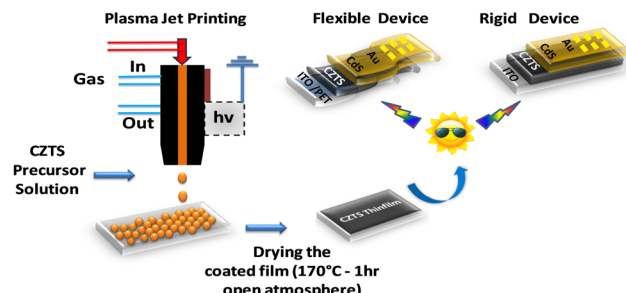


Fig. 1 APPJ printing of CZTS for the fabrication of solar cells on rigid and flexible substrates.

2.4. Characterization

The structural characteristics of the film were investigated using X-ray diffraction (XRD) (PANalytical X'pert powder diffractometer) with Cu K α radiation. Raman analysis (Horiba Jobin-Yvon Lab-Ram HR) was performed using an Ar $^+$ laser with a 473 nm line as the excitation source. Silicon was used to calibrate the instrument at 520.7 cm $^{-1}$. UV-visible spectroscopy was carried out using JASCO UV-vis spectrophotometer. The composition and surface morphology of the film were studied by SEM-EDS (Zeiss Supra 55-VP FEGSEM). Elemental analysis was performed using X-ray photoelectron spectroscopy (Kratos XSAM 800), equipped with a dual-anode X-ray source, where Mg K α (1253.6 eV) was used for these studies. A transmission electron microscopy (TEM) study of the as-prepared sample was carried out using the JEOL JEM-2100. The semiconducting properties were studied using a Hall effect setup (Ecopia HMS Ver 3.51:3). The J - V (current density–voltage) characteristics of the devices were measured using a Keithley 2400 source-measure unit. To obtain the 1 sun AM 1.5G illumination, an Oriel Sol3A Class AAA solar simulator was employed.

2.5. Device fabrication and testing

The ITO-coated glass substrate (8–12 Ω cm $^{-2}$) was ultrasonicated for 10 min in DI water, ethanol, and isopropanol (IPA), and then dried with nitrogen gas. The precursor solution of CZTS was then deposited onto the ITO substrate using APPJ. A 60 nm CdS layer (n-type) was deposited *via* spin coating onto the CZTS film.⁴² Then, using a shadow mask, Au top contacts (\sim 100 nm thick) were thermally evaporated under vacuum (10^{-6} torr). The device active area was 0.24 cm 2 . A similar procedure was followed for the fabrication of the device on PET/ITO substrates.

3. Results and discussion

The structural and chemical analyses of APPJ-printed and dip-coated CZTS films were performed while optimizing the precursor solution concentration and processing conditions. Raman analysis clearly showed that a few secondary phases, such as Cu_{Sn}S and CuS, were present in the film APPJ-printed using the as-prepared precursor solution (Fig. S4a, ESI †). Annealing trials were conducted at (i) 130 °C and (ii) 170 °C for 1 h in open atmosphere. No secondary phases were

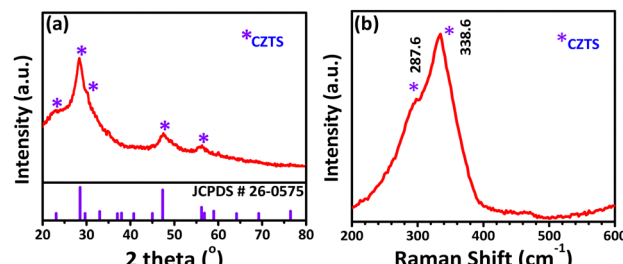


Fig. 2 (a) XRD spectrum and (b) Raman spectrum of the APPJ-printed CZTS film processed with optimized conditions.

observed in the film prepared using the 50% diluted solution and annealed at 170 °C for 1 h (Fig. S4b, ESI †). As shown in Fig. 2(a), the XRD pattern of the APPJ-printed CZTS film dried at 170 °C for 1 h showed major peaks at $2\theta = 56.1^\circ$, 47.3° , and 28.5° , corresponding to the (312), (220), and (112) planes of the kesterite CZTS phase, respectively.⁵⁶ The calculated crystallite size was \sim 0.32 nm along the (112) plane,⁵⁷ which was close to values reported in the literature and was further confirmed by the TEM results (Fig. 4). The formation of the CZTS film was confirmed by the Raman spectrum shown in Fig. 2(b). The spectrum showed an intense peak at 338 cm $^{-1}$, along with a shoulder at 287 cm $^{-1}$, both corresponding to the CZTS phase. The XRD and Raman spectra revealed that the initial phase of CZTS growth was likely amorphous, as the process occurs at a relatively low temperature of 170 °C for 1 h. Moreover, the UV-visible absorption spectra of the APPJ-printed film showed absorption in the visible region (Fig. S6 and S8, ESI †), with a calculated optical bandgap of 1.50 eV. This bandgap value was in good agreement with literature reports on CZTS.⁵⁶ Notably, The APPJ-printed CZTS film exhibited a higher absorption coefficient compared to the dip-coated CZTS film (Fig. S8, ESI †), possibly due to differences in crystallite size and improved microstructure.

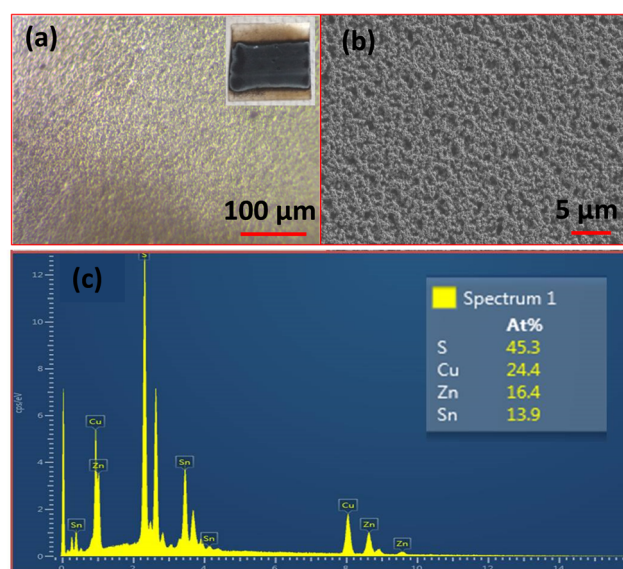


Fig. 3 (a) Optical image (inset: Photograph of the CZTS film), (b) FESEM image, and (c) EDS analysis of the APPJ-printed CZTS film.



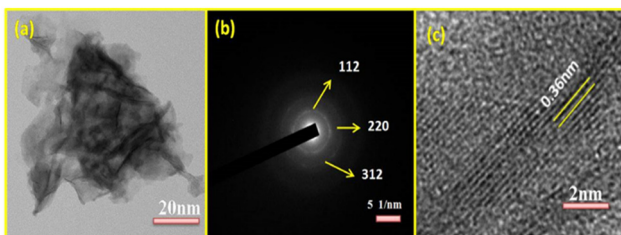


Fig. 4 (a) TEM image, (b) selected-area electron diffraction (SAED) pattern, and (c) HRTEM image of the APPJ-printed CZTS film.

Fig. 3 shows the optical and FESEM images of the APPJ-printed CZTS film. The surface of the film was more compact and denser compared to the film prepared *via* the dip-coating route (Fig. S5, ESI†). This could be attributed to the smaller particle size of the APPJ-printed CZTS film (~ 250 nm) compared to that of the dip-coated CZTS film (~ 550 nm).

Furthermore, the chemical composition estimated from EDS analysis was close to the expected stoichiometry of CZTS. Interestingly, the TEM image of the APPJ-printed CZTS film sample revealed a sheet-like structure, as shown in Fig. 4(a). A similar flake-like structure was also observed in the TEM image of the dip-coated CZTS sample (Fig. S7, ESI†). The SAED patterns in Fig. 4(b) and Fig. S7(b) (ESI†) confirmed the crystalline nature of the APPJ-printed and dip-coated CZTS films. HRTEM images further confirmed interplanar spacings of 0.36 nm (APPJ-printed CZTS) and 0.32 nm (dip-coated CZTS), corresponding to the (112) planes of tetragonal CZTS (Fig. 4(c) and Fig S7(c), ESI†). Upon measuring the charge carrier density of these films using Hall Effect, the plasma-printed CZTS films exhibited p-type semiconducting behavior. The estimated carrier mobility of the APPJ-printed CZTS film was higher than that reported in earlier studies and higher than that of the dip-coated CZTS film,^{58–60} as it was more porous and compact

Table 1 Hall effect measurement results of the CZTS thin film compared with those from other literature

Method	Carrier concentration (ρ) cm^{-3}	Mobility (μ_H) $\text{cm}^2 \text{V}^{-1} \text{s}^{-1}$	Hall coefficient (R_H) $\text{cm}^3 \text{C}^{-1}$	Resistivity (ρ) Ωcm^{-1}	Conductivity type	Ref.
Atmospheric plasma	4.8×10^{20}	5.8	8.8×10^3	1.1×10^{-2}	p	This work
Dip-coating	2.7×10^{20}	3.2	8.0×10^3	1.2×10^{-2}	p	This work
Doctor blade	1.24×10^{16}	16.57	30.22	—	p	58
Plasma-assisted co-evaporation	2.6×10^{19}	2.3	—	1.0×10^{-1}	p	59
dc sputtering	2.5×10^{19}	1.2	2.4×10^{-1}	1.8×10^{-1}	p	60

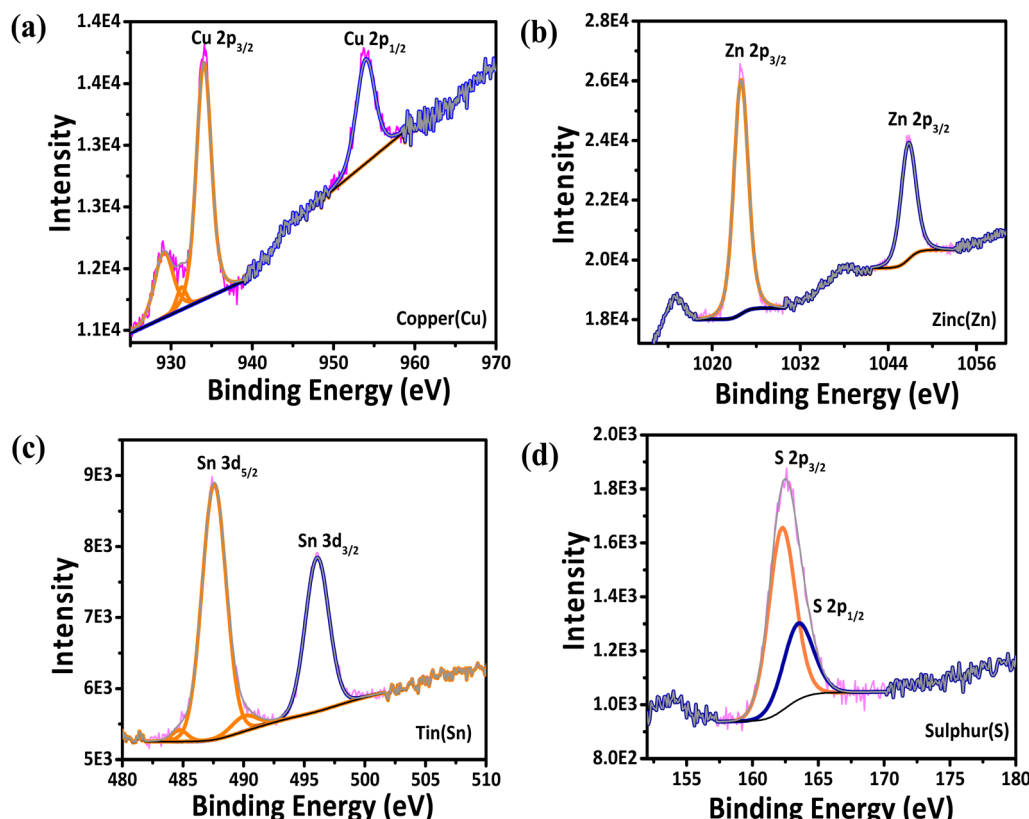


Fig. 5 XPS Spectra of (a) Cu 2p, (b) Zn 2p, (c) Sn 3d, and (d) S 2p spectra of the APPJ-printed CZTS film.



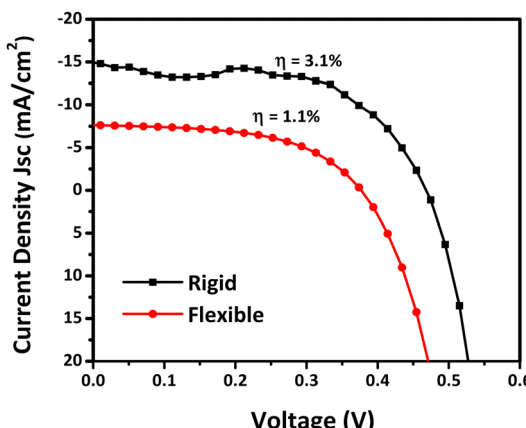


Fig. 6 J – V curves of the APPJ-printed CZTS-based solar cells on rigid and flexible substrates, measured under light illumination (100 mW cm^{-2} , AM 1.5).

(Fig. 4(b)). Interestingly, the carrier concentration and Hall coefficient were also higher compared to previous works^{58–60} (Table 1). The observed resistivity was slightly lower than that of the dip-coated film, which may be attributed to the improved crystallinity and density of the APPJ-printed CZTS.³¹

The wide scan survey XPS spectrum of the APPJ-printed film confirmed the presence of all elements expected for CZTS (Fig. S9, ESI†). From the XPS analysis, the binding energies of 934 eV for Cu 2p_{3/2} and 954 eV for Cu 2p_{1/2}, with a 20 eV peak splitting, are shown in Fig. 5(a). At higher binding energies, no satellite peaks were observed, indicating that the Cu²⁺ present in the starting material of CZTS had been reduced to monovalent copper. Fig. 5(b) shows the peaks at 1024 eV for Zn 2p_{3/2} and 1046.7 eV of Zn 2p_{1/2}, with a 22.7 eV peak splitting. These values corresponded well with the standard divalent Zn(II) splitting. The two peaks at 487.6 eV and 496 eV, with a wide peak splitting of 8.4 eV, were attributed to the oxidation of Sn²⁺ in the starting material to Sn⁴⁺ (Fig. 5(c)). The two peaks located at 162.3 eV and 163.6 eV (Fig. 5(d)) were assigned to the S 2p core levels in the sulfide phases, which typically appear in this region according to the literature.⁶¹

3.1. Heterojunction device fabrication and characterization

Simple heterojunction solar cells were fabricated with both APPJ-printed and dip-coated CZTS films in the configuration ITO/CZTS/CdS/Au, using rigid glass and flexible PET substrates. The J – V characteristics of the APPJ-printed CZTS solar cell device under light illumination are shown in Fig. 6. The device on the rigid substrate exhibited a PCE (η) of 3.1%, a short-circuit current density (J_{sc}) of 14.5 mA cm^{-2} , an open-circuit voltage (V_{oc}) of 0.47 V, and a fill factor (FF) of 0.46. The solar cell on the flexible PET substrate exhibited a η of 1.1%, a V_{oc} of 0.37 V, a J_{sc} of 7.5 mA cm^{-2} , and an FF of 0.41. In comparison to earlier reports on low-temperature processed CZTS-based solar cells, the efficiency of the APPJ-printed CZTS was superior, with a high value of J_{sc} (Table 2). This could be attributed to the enhanced light absorption, porous nature, and mobility, as confirmed through characterization techniques (UV visible spectra, XRD spectra, and Hall

Table 2 Comparison of photovoltaic characteristics of heterojunction devices based on low temperature processed CZTS films

Device structure	Coating method of CZTS film	Processing conditions of CZTS film	V_{oc} (V), J_{sc} (mA cm^{-2}), FF	η (%)	Device area (cm^2)	Ref.
PI/Mo/CZTS/CdS/ZnO/AI	Screen printing	Drying for 1 h (open air), hot pressed using a hot roll at 195 °C (open air)	0.38, 4.76, 0.27	0.49	0.15	31
SLG/ITO–CZTS–PCBM–Ca/Al	Spin-coating	Drying in open air (temperature not mentioned)	0.39, 5.30, 0.43	0.90	0.04	62
SLG/FTO/TiO ₂ /CdS/CZTS/Graphite	Spray pyrolysis	Drying at 140 °C for 30 min (N ₂) and annealed at 300 °C for 30 min (N ₂)	445, 6.7, 37.4, 0.43	0.43	—	63
SLG/FTO/TiO ₂ /CdS/CZTS/Carbon paste	Spray pyrolysis	Drying at 140 °C for 30 min (N ₂) and annealed at 250 °C for 30 min (N ₂)	502, 2.8, 36	0.51	—	64
SLG/ITO/ZnO/CdS/CZTS/Au	Spin coating	Drying at 150 °C for 10 min (open air) and annealed at 250 °C for 10 min (open air)	0.67, 4.10, 0.43	1.20	0.12	65
SLG/ITO/CZTS/CdS/Al	Spin-coating	Annealed at 350 °C for 5 min	0.40, 3.56, 54.90	0.78	0.32	42
SLG/ITO/CZTS/CdS/Al	Dip-coating	Drying at 130 °C for 15 min and annealing at 100 °C for 2.5 h (Ar)	0.52, 11.2, 0.47	2.73	0.24	46
PET/ITO/CZTS/CdS/Al	Dip-coating	Drying at 130 °C for 15 min and annealing at 100 °C for 2.5 h (Ar)	0.48, 2.2, 0.71	0.74	0.24	46
SLG/ITO/CZTS/CdS/Au	Dip-coating	Drying at 130 °C for 15 min (open air) and annealing at 100 °C for 2.5 h (Ar)	0.42, 11.6, 0.49	2.38	0.24	This work
PET/ITO/CZTS/CdS/Au	Dip-coating	Drying at 130 °C for 15 min (open air) and annealing at 100 °C for 2.5 h (Ar)	0.33, 5.41, 0.29	0.51	0.24	This work
SLG//ITO/CZTS/CdS/Au	APPJ	Annealing at 170 °C for 1 h (open air)	0.47, 14.5, 0.46	3.1	0.24	This work
PET//ITO/CZTS/CdS/Au	APPJ	Annealing at 170 °C for 1 h (open air)	0.37, 7.5, 0.41	1.1	0.24	This work

measurements). The *J*-*V* curves of the dip-coated CZTS-based solar cells on rigid and flexible substrates, measured under both dark and light illumination, are shown in Fig. S10 (ESI[†]). The *V*_{oc} was slightly lower than that of the dip-coated CZTS film, indicating relatively more charge recombination in the APPJ-printed CZTS. This was plausible, as recombination was directly proportional to the carrier concentration, which was found to be higher in the APPJ-printed CZTS film compared to the dip-coated film (Table 2).

Thus, this work demonstrates a one-step deposition process for CZTS using the APPJ technique. It is a low-temperature, eco-friendly approach that utilizes less toxic solvents. These unique features have the potential to drive significant advancements in the scalable, environmentally sustainable fabrication of CZTS-based solar cells.

4. Conclusion

In summary, we confirmed the open-air formation of a nanocrystalline, high-quality CZTS film on rigid as well as flexible substrates at low temperature (~ 170 °C) using the APPJ printing route. In comparison with the dip-coated film annealed under an Ar atmosphere, the APPJ-printed CZTS film exhibited superior quality, a higher absorption coefficient, and higher carrier concentration. The fabricated glass/ITO/CZTS/CdS/Au and PET/ITO/CZTS/CdS/Au heterojunction solar cell devices demonstrated PCEs of 3.1% and 1.1%, respectively, which are the highest reported to date for low-temperature-processed CZTS. Demonstrated with CZTS, this new approach employing APPJ printing of the precursor solution may potentially enable the scalable, low-temperature fabrication of high-quality chalcogenide thin films for various applications, including flexible photovoltaics, thermoelectrics, and photo-electrochemical devices.

Data availability

The data supporting this article have been included as part of the ESI.[†]

Conflicts of interest

There are no conflicts to declare.

Acknowledgements

The authors acknowledge the grant from the International Research Exchange Scheme (IES|R2\170272), The Royal Society, UK, towards this research work. The authors also thank SRM IST, Kattankulathur, Tamil Nadu, India, The Open University, UK, DST-SERB (ECR/2015/000513) and MNRE (31/03/2014-15/PVSE-R&D) for the support and funding extended. They are grateful to IIT SAIF for extending the FESEM facility and to Dr Ramesh Babu of Bharathidhasan University, Trichy, for assistance with Hall measurements. Special thanks to the Indian National Users Program (INUP) at IISc CeNSE Bangalore for

providing facilities, such as cross-sectional FESEM imaging, solar simulator, and IV measurements. M. D. thanks CSIR for the senior research fellowship.

References

- M. Graetzel, R. A. J. Janssen, D. B. Mitzi and E. H. Sargent, *Nature*, 2012, **488**, 304–312.
- S. E. Habas, H. A. S. Platt, M. F. A. M. van Hest and D. S. Ginley, *Chem. Rev.*, 2010, **110**, 6571–6594.
- D. B. Mitzi, O. Gunawan, T. K. Todorov, K. Wang and S. Guha, *Sol. Energy Mater. Sol. Cells*, 2011, **95**, 1421–1436.
- K. Ramasamy, M. A. Malik and P. O'Brien, *Chem. Commun.*, 2012, **48**, 5703.
- H. Katagiri, K. Jimbo, W. S. Maw, K. Oishi, M. Yamazaki, H. Araki and A. Takeuchi, *Thin Solid Films*, 2009, **517**, 2455–2460.
- Y. Li, C. Cui, H. Wei, Z. Shao, Z. Wu, S. Zhang, X. Wang, S. Pang and G. Cui, *Adv. Mater.*, 2024, **36**, 2400138.
- R. Nitsche, D. F. Sargent and P. Wild, *J. Cryst. Growth*, 1967, **1**, 52–53.
- K. Ito and T. Nakazawa, *Jpn. J. Appl. Phys.*, 1988, **27**, 2094.
- H. Katagiri, N. Sasaguchi, S. Hando, S. Hoshino, J. Ohashi and T. Yokota, *Sol. Energy Mater. Sol. Cells*, 1997, **49**, 407–414.
- W. Shockley, *Solid State Electron.*, 1961, **2**, 35–67.
- W. Wang, M. T. Winkler, O. Gunawan, T. Gokmen, T. K. Todorov, Y. Zhu and D. B. Mitzi, *Adv. Energy Mater.*, 2014, **4**, 1301465.
- B. Shin, O. Gunawan, Y. Zhu, N. A. Bojarczuk, S. J. Chey and S. Guha, *Prog. Photovoltaics Res. Appl.*, 2013, **21**, 72–76.
- Y. S. Lee, T. Gershon, O. Gunawan, T. K. Todorov, T. Gokmen, Y. Virgus and S. Guha, *Adv. Energy Mater.*, 2015, **5**, 2–5.
- S. Ahmed, K. B. Reuter, O. Gunawan, L. Guo, L. T. Romankiw and H. Deligianni, *Adv. Energy Mater.*, 2012, **2**, 253–259.
- J. J. Scragg, T. Ericson, X. Fontané, V. Izquierdo-Roca, A. Pérez-Rodríguez, T. Kubart, M. Edoff and C. Platzer-Björkman, *Prog. Photovoltaics Res. Appl.*, 2014, **22**, 10–17.
- J. Zhong, Z. Xia, C. Zhang, B. Li, X. Liu, Y.-B. Cheng and J. Tang, *Chem. Mater.*, 2014, **26**, 3573–3578.
- T. K. Todorov, K. B. Reuter and D. B. Mitzi, *Adv. Mater.*, 2010, **22**, E156–E159.
- C. Steinhagen, T. B. Harvey, C. J. Stolle, J. Harris and B. A. Korgel, *J. Phys. Chem. Lett.*, 2012, **3**, 2352–2356.
- M. H. Kumar, N. Yantara, S. Dharani, M. Graetzel, S. Mhaisalkar, P. P. Boix and N. Mathews, *Chem. Commun.*, 2013, **49**, 11089.
- G. Choudhary and H. Hansen, *Chemosphere*, 1998, **37**, 801–843.
- F. J. C. Roe, G. A. Grant and D. M. Milican, *Nat. Publ. Gr.*, 1967, **216**, 375–376.
- T. Schnabel, M. Löw and E. Ahlswede, *Sol. Energy Mater. Sol. Cells*, 2013, **117**, 324–328.



23 G. Wang, W. Zhao, Y. Cui, Q. Tian, S. Gao, L. Huang and D. Pan, *ACS Appl. Mater. Interfaces*, 2013, **5**, 10042–10047.

24 F. Liu, S. Shen, F. Zhou, N. Song, X. Wen, J. A. Stride, K. Sun, C. Yan and X. Hao, *J. Mater. Chem. C*, 2015, **3**, 10783–10792.

25 G. L. Agawane, A. S. Kamble, S. A. Vanalakar, S. W. Shin, M. G. Gang, J. H. Yun, J. Gwak, A. V. Moholkar and J. H. Kim, *Mater. Lett.*, 2015, **158**, 58–61.

26 V. Tunuguntla, W.-C. Chen, P.-H. Shih, I. Shown, Y.-R. Lin, J.-S. Hwang, C.-H. Lee, L.-C. Chen and K.-H. Chen, *J. Mater. Chem. A*, 2015, **3**, 15324–15330.

27 C. Steinhagen, M. G. Panthani, V. Akhavan, B. Goodfellow, B. Koo and B. A. Korgel, *J. Am. Chem. Soc.*, 2009, **131**, 12554–12555.

28 D. Payno, S. Kazim, M. Salado and S. Ahmad, *Sol. Energy*, 2021, **224**, 1136–1143.

29 L. Dong, S. Cheng, Y. Lai, H. Zhang and H. Jia, *Thin Solid Films*, 2017, **626**, 168–172.

30 Q. Tian, X. Xu, L. Han, M. Tang, R. Zou, Z. Chen, M. Yu, J. Yang and J. Hu, *CrystEngComm*, 2012, **14**, 3847.

31 Z. Zhou, Y. Wang, D. Xu and Y. Zhang, *Sol. Energy Mater. Sol. Cells*, 2010, **94**, 2042–2045.

32 I. Becerril-Romero, L. Acebo, F. Oliva, V. Izquierdo-Roca, S. López-Marino, M. Espíndola-Rodríguez, M. Neuschitzer, Y. Sánchez, M. Placidi, A. Pérez-Rodríguez, E. Saucedo and P. Pistor, *Prog. Photovoltaics Res. Appl.*, 2018, **26**, 55–68.

33 Q. Zhao, H. Shen, K. Gao, Y. Xu, X. Wang and Y. Li, *J. Mater. Chem. C*, 2021, **9**, 17531–17541.

34 K. W. Brew, S. M. McLeod, S. M. Garner and R. Agrawal, *Thin Solid Films*, 2017, **642**, 110–116.

35 F. Fu, T. Feurer, T. Jäger, E. Avancini, B. Bissig, S. Yoon, S. Buecheler and A. N. Tiwari, *Nat. Commun.*, 2015, **6**, 1–9.

36 X. Mathew, J. P. Enriquez, A. Romeo and A. N. Tiwari, *Sol. Energy*, 2004, **77**, 831–838.

37 J. Ramanujam and U. P. Singh, *Energy Environ. Sci.*, 2017, **10**, 1306–1319.

38 V. V. Satale and S. V. Bhat, *Sol. Energy*, 2020, **208**, 220–226.

39 S. Sun, T. Salim, N. Mathews, M. Duchamp, C. Boothroyd, G. Xing, T. C. Sum and Y. M. Lam, *Energy Environ. Sci.*, 2014, **7**, 399–407.

40 Z. Xu, T. Li, F. Zhang, X. Hong, S. Xie, M. Ye, W. Guo and X. Liu, *Nanoscale*, 2017, **9**, 3826–3833.

41 Z. Gao, W. Jin, Y. Li, Q. Song, Y. Wang, K. Zhang, S. Wang and L. Dai, *J. Mater. Chem. C*, 2015, **3**, 4511–4514.

42 Y. Hou, H. Azimi, N. Gasparini, M. Salvador, W. Chen, L. S. Khanzada, M. Brandl, R. Hock and C. J. Brabec, *ACS Appl. Mater. Interfaces*, 2015, **7**, 21100–21106.

43 M. A. Islam, K. S. Rahman, F. Haque, M. Akhtaruzzaman, M. M. Alam, Z. A. Alothman, K. Sopian and N. Amin, *Chalcogenide Lett.*, 2014, **11**, 233–239.

44 M. Farinella, R. Inguanta, T. Spanò, P. Livreri, S. Piazza and C. Sunseri, *Energy Procedia*, 2014, **44**, 105–110.

45 U. Saha and M. K. Alam, *RSC Adv.*, 2018, **8**, 4905–4913.

46 M. Dhanasekar and S. V. Bhat, *2020 47th IEEE Photovoltaic Specialists Conference (PVSC)*, IEEE, 2020, pp. 1–3.

47 M. Dhanasekar, PhD thesis, SRM University, 2020.

48 G. Cummins and M. P. Y. Desmulliez, *Circuit World*, 2012, **38**, 193–213.

49 J. M. Hoey, A. Lutfurakhmanov, D. L. Schulz and I. S. Akhatov, *J. Nanotechnol.*, 2012, **2012**, 1–22.

50 X. Lu, G. V. Naidis, M. Laroussi and K. Ostrikov, *Phys. Rep.*, 2014, **540**, 123–166.

51 K. Ostrikov, E. C. Neyts and M. Meyyappan, *Adv. Phys.*, 2013, **62**, 113–224.

52 A. Dey, S. Krishnamurthy, J. Bowen, D. Nordlund, M. Meyyappan and R. P. Gandhiraman, *ACS Nano*, 2018, **12**, 5473–5481.

53 M. Bhar, A. Dey, S. Ghosh, M. A. van Spronsen, V. Selvaraj, Y. Kaliprasad, S. Krishnamurthy and S. K. Martha, *Carbon*, 2022, **198**, 401–410.

54 M. Dhanasekar, S. Sekar and S. V. Bhat, *J. Colloid Interface Sci.*, 2021, **599**, 326–331.

55 M. Dhanasekar and S. V. Bhat, *Appl. Surf. Sci.*, 2017, **418**, 194–198.

56 S. K. Swami, A. Kumar and V. Dutta, *Energy Procedia*, 2013, **33**, 198–202.

57 J. Wang, P. Zhang, X. Song and L. Gao, *RSC Adv.*, 2014, **4**, 27805–27810.

58 D. Tang, Q. Wang, F. Liu, L. Zhao, Z. Han, K. Sun, Y. Lai, J. Li and Y. Liu, *Surf. Coat. Technol.*, 2013, **232**, 53–59.

59 Y. Li, J. Chen and J. Ma, *J. Mater. Sci.: Mater. Electron.*, 2015, **26**, 6546–6551.

60 N. Muhunthan, O. P. Singh, M. K. Thakur, P. Karthikeyan, D. Singh, M. Saravanan and V. N. Singh, *J. Sol. Energy*, 2014, **2014**, 1–8.

61 Y. Sun, Y. Zhang, H. Wang, M. Xie, K. Zong, H. Zheng, Y. Shu, J. Liu, H. Yan, M. Zhu and W. Lau, *J. Mater. Chem. A*, 2013, **1**, 6880.

62 S. K. Saha, A. Guchhait and A. J. Pal, *Phys. Chem. Chem. Phys.*, 2012, **14**, 8090.

63 K. Tanaka, M. Kurokawa, K. Moriya and H. Uchiki, *J. Alloys Compd.*, 2013, **571**, 98–102.

64 M. Kurokawa, K. Tanaka, K. Moriya and H. Uchiki, *Jpn. J. Appl. Phys.*, 2012, **51**, 10NC33.

65 D. Lee and K. Yong, *Nanotechnology*, 2014, **25**, 065401.

